Proceeding of the 13th National Mechanical Engineering Conference
2-3 December 1999, Royal Cliff Beach Resort Hotel, South Pattaya, Cholburi

A Comparative Study of Flux-Limiters in Unsteady and Steady Flows

V. Suratanakavikul
Computational Mechanics Laboratory (CML),
Department of Mechanical Engineering, Faculty of Engineering,
Kasetsart University, Bang-khen, Bangkok 10900
Phone 66(2)9428555, Fax. 66(2)5794576, E-Mail: ovrsk@ku.ac.th

A. J. Marquis
Department of Mechanical Engineering, Imperial College,
Exhibition Road, London, SW 7 2BX, England

Abstract

A comparative study of a number of flux-limiters is presented in this paper to find the most suitable flux-limiter to be used in unsteady and steady convective flow calculations. The accuracy and convergence behaviour of these flux-limiters are assessed in five pure convection problems: (1) rotation of a cone-shaped scalar field, (2) advection of a square-shaped scalar field, (3) mixing of a hot with a cold front, (4) deformation of cone-shaped scalar field and (5) IAHR. The *superbee* flux-limiter is the most accurate in unsteady flow problems although the *Koren* flux-limiter is more appropriate in steady flow problems because of its good convergence behaviour.

1. Introduction

In general, convective terms in the governing equations can be discretised using various differencing schemes such as Central Differencing (CD), First-Order Upwind (FOU), Second-Order Upwind (SOU) and Second-Order-Limited Upwind (SOLU) differencing schemes. The solutions obtained using FOU are always bounded and appear to be more physically realistic than those using CD although the results are diffusive; while SOU gives more accurate results than FOU but the results may exceed realistic bounds.

The SOLU scheme is the most appropriate to be used in discretising convective terms due to a non-linear function called a flux -limiter that was initiall introduced by van Leer [1, 2] to prevent the unwanted oscillations and to ensure that the results are physicall realistic (bounded), i.e. the flux-limiter is used to limit the amplitude of the gradient appearing in the original second-order difference equation, by multiplying the flux terms in the difference equations with these so called flux-limiters.

The purpose of this paper is to compare the accuracy and convergence behaviour of five different flux-limiters: *van Leer, minmod, superbee, MUSCL, Koren* basing on a Second-Order-Limited Upwind (SOLU) scheme in five pure convection test cases. Five pure convection problems (four unsteady, one steady) considered in this work are (i) rotation of a scalar cone, (ii) transport of a scalar square, (iii) mixing of a hot with a cold front, (iv) deformation of a scalar cone and (v) the IAHR problem.

2. Mathematical Formulation

2.1 Governing Equations

The following pure convection equation is considered in order to examine the performance of the second-order-limited upwind differencing scheme in discretising convective term.

$$\left(\frac{\partial \phi}{\partial t}\right)+\left(\frac{\partial u\phi}{\partial x}\right)+\left(\frac{\partial v\phi}{\partial y}\right)=0 \qquad (1)$$

where ϕ is a scalar function of two space dimensions and time, u and v are the two components of the velocity vector.

2.2 Second-Order-Limited Upwind Differencing Schem

For simplicity, only steady one-dimensional flow is considered here. The governing equation is composed of convective and diffusive terms in the x-direction only.

$$\frac{d}{dx}(\rho u\phi)=\frac{d}{dx}(\Gamma\frac{d\phi}{dx}) \qquad (2)$$

In Fig. 1, node P is typically used to represent a centre point of the control volume. Nodes W and E are located to the west and east of node P respectively and the west and east faces of the control volume are identified by the lower-case letters w and e, Versteeg [1].

The resulting equation after the integration of equation (2) over the control volume of Fig. 1 is

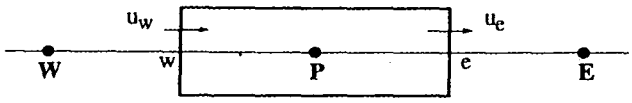

Fig. 1 A Control Volume around Node P

$$(\rho u A\phi)_e - (\rho u A\phi)_w = \left(\Gamma A \frac{\partial \phi}{\partial x}\right)_e - \left(\Gamma A \frac{\partial \phi}{\partial x}\right)_w \quad (3)$$

If the convective mass flux per unit area and diffusion conductance are identified as F = ρu and D = Γ/δx respectively, the diffusion term on the right hand side of equation (3) are discretised using the central differencing scheme and the areas at the east and west faces of the control volume are assumed to be equal, the discretised form of equation (2) can be written as

$$F_e\phi_e - F_w\phi_w = D_e(\phi_E - \phi_P) - D_w(\phi_P - \phi_W) \quad (4)$$

The velocity field and hence the mass flux at the east and west faces (F_e and F_w) are assumed to be known. Differencing schemes are used, essentially, to obtain the transported propert ϕ at the east and west faces of the control volume, i.e. ϕ_e and ϕ_w, in terms of the noded values ϕ_P, ϕ_E and ϕ_W. If the second-order-limited upwind differencing scheme is used and u_e and u_w are positive, ϕ_e and ϕ_w can be expressed as

$$\phi_e = \phi_P + \frac{\psi_e}{2}(\phi_E - \phi_P) \quad (5)$$

$$\phi_w = \phi_W + \frac{\psi_w}{2}(\phi_P - \phi_W) \quad (6)$$

where ψ is a flux limiter. The distribution of the considered flux limiters, ψ, against consecutive gradient, r, are plotted and presented in Table 1, where r is the consecutive gradient defined as

$$r = \frac{\phi_D - \phi_C}{\phi_C - \phi_U} \quad (7)$$

where ϕ_D, ϕ_C and ϕ_U represent downstream, centre and upwind values respectively.

The discretised form of the general transport equation can then be written as

$$a_P\phi_P^{n+1} = \sum_{\alpha=E,W} a_\alpha\phi_\alpha^{n+1} + b_P \quad (8)$$

where

$$a_P = \sum_{\alpha=E,W} a_\alpha \quad (9)$$

$$b_P = S_\phi^{DC} \quad (10)$$

and the coefficients, a_α, are evaluated at time step n, and are expressed as

$$aw = D_w + \max(F_w, 0) \quad (11)$$

$$a_E = D_e + \max(0, -F_e) \quad (12)$$

S_ϕ^{DC} is an additional source term resulting from the flux-limiter.

$$S_\phi^{DC} = F_e\left\{\frac{\psi_e}{2}(\phi_E - \phi_P)\right\} - F_w\left\{\frac{\psi_w}{2}(\phi_P - \phi_W)\right\} \quad (13)$$

The time marching in the case of the unsteady problems, is performed using an explicit 4 th order accurate Runge-Kutta scheme [2]. For steady flow problems, the solutions can be obtained either by calculating forward in time for a sufficiently long period or, alternatively by omitting the transient term and then solving the equations iteratively. The former case is adopted in this work.

3. Results and Discussion

In order to examine and compare the ability of different flux-limiters in capturing the steep gradient and discontinuities, the maximum and minimu solution values from each test case are tabulated and the scalar contours are plotted on the selected grid in this section. The scalar contour plots of *minmod* and *superbee* are presented to represent the flux-limiters that give the least and the most accurate results respectively, and the scalar contour plots of *Koren* are presented because of its good convergence behaviour and accurate results.

3.1 Rotation of a Cone-Shaped Scalar Field

This test case is chosen to test ability of each differencing scheme in capturing steep gradients. A scalar "cone" field is advected around by a steady velocity field and is defined by the initial conditions.

$$\phi(x, y) = 5\left\{1 + \cos\left(\frac{r\pi}{r_c}\right)\right\} \quad \text{if } r \le r_c$$

otherwise; $\phi(x, y) = 0$ (14)

The domain is $x \ge -0.5$, $y \le 0.5$ and the cone is centered originally at $(x_0, y_0) = (0.0, 0.25)$ and a radius of the cone, $r_c = 0.1$. The distance from the cone centre r is,

$$r = \sqrt{(x - x_o)^2 + (y - y_o)^2} \quad (15)$$

The velocity field revolve counterclockwise about (0,0) with angular velocity $\omega = 2.0$ rad/sec and is given by

$$u(x, y) = -2y$$
$$v(x, y) = 2x \qquad (16)$$

A time step equal to 0.005 is used because the results using the time step ≤ 0.005 are not different, i.e. the results are independent of time step, and for one full rotation of the cone around the centre of the domain this results in 628 time steps. The maximum and minimum values of the results for three grids of 16x16, 32x32 and 64x64 nodes are presented in Table 2 and three-dimensional perspective plots of the results observed on the grid 32x32 are shown in Fig. 2.

The predicted maximum and minimum field value from each flux-limiter in Table 2 indicate that the *superbee* flux-limiter predicts the highest and the *minmod* flux-limiter predicts the lowest maximum value respectively. This agrees with the 3D perspective plot in Fig. 2 that the steep gradients of scalar field are very well captured by the *superbee* and *Koren* flux-limiters while the *minmod* scheme results in more diffusive results. It should be noted that the plots of the results from the Second-Order-Limited Upwind (SOLU) schemes show that the results are less diffusive than the First-Order Upwind (FOU) scheme and also the results are bounded. This is as expected from the literature. Another point that should be mentioned from the table is that the predicted minimum scalar field value is less than zero for all flux-limiters except *minmod*. Although the predicted negative values are very small a problem may arise in the case where the positive-definite values are important e.g. heat transfer problem.

Table 1 Flux Limiters

van Leer [3]: $\psi(r) = \dfrac{r+\lvert r\rvert}{1+r}$	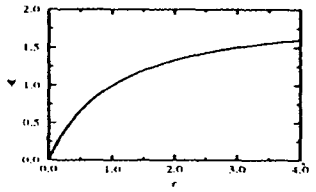
minmod [4]: $\psi(r) = \max[0, \min(r,1)]$	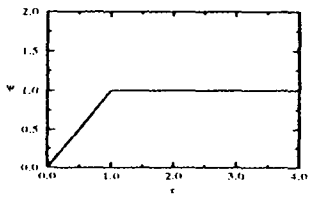
superbee [5]: $\psi(r) = \max[0, \min(2r,1), \min(r,2)]$	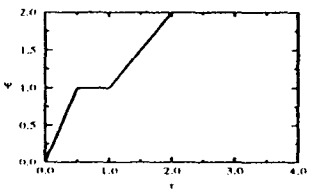
MUSCL [6]: $\psi(r) = \max\left[0, \min\left(2r, \dfrac{1}{2}+\dfrac{1}{2}r, 2\right)\right]$	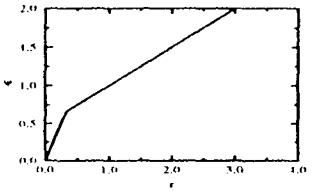
Koren [7]: $\psi(r) = \max\left[0, \min\left(2r, \dfrac{2}{3}r+\dfrac{1}{3}, 2\right)\right]$	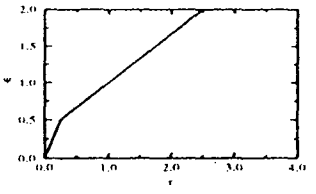

Table 2 The Maximum and Minimum Field Values of the Revolving Cone Problem

	16x16		32x32		64x64	
	max	min	max	min	max	min
FOU	0.38	1.81×10^{-12}	0.75	0.00	1.44	6.11×10^{-17}
SOLU:						
van Leer	0.97	-1.37×10^{-15}	2.58	-2.17×10^{-15}	5.74	-2.26×10^{-14}
minmod	0.75	1.56×10^{-13}	1.85	0.00	4.07	7.09×10^{-28}
superbee	1.27	-2.15×10^{-7}	3.81	-6.05×10^{-7}	8.17	-4.54×10^{-6}
MUSCL	1.09	-4.65×10^{-8}	3.01	-1.60×10^{-7}	6.58	-9.70×10^{-7}
Koren	1.09	-3.28×10^{-8}	3.05	-1.28×10^{-7}	6.79	-6.06×10^{-7}

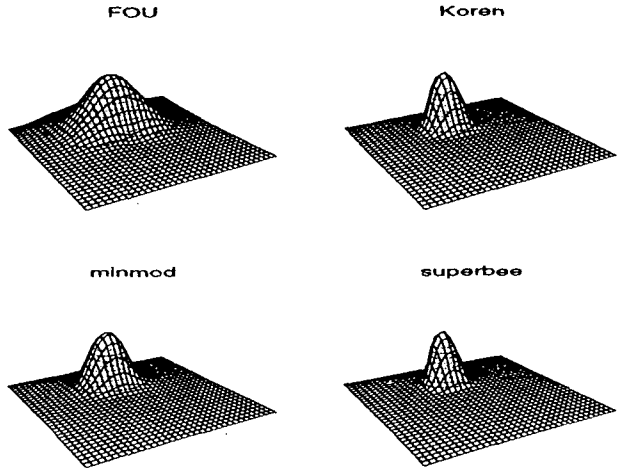

Fig. 2 The 3-D Perspective Plots of the Revolving Cone Problem

3.2 Advection of a Square-Shaped Scalar Field

The present test case is chosen to test the ability of the differencing schemes in the problems with greater discontinuities than the previous test case. In this test case, a square scalar field is advected by a unifor velocity field and the initial conditions are

$$\phi(x,y)=10 \quad \text{if}$$

$$(|x-x_0|,|y-y_0|)\le\frac{a}{2}$$

$$\text{otherwise;}\quad \phi(x,y)=0 \tag{17}$$

The co-ordinates of the centre of the square are, initiall , at $(x_0, y_0) = (-1.5, -1.5)$ and the width of the square is a = 1.5. The domain of the problem is $x \ge -3$, $y \le 3$. The velocity field is steady with two velocit components equal to unity. The solutions are time-independent for $\delta t = 0.02$ and advanced for 140 time steps which correspond to the square field being advected for a length equal to 3.95 units from the initial location towards the opposite corner of the domain.

The results are predicted on regular meshes of 20x20, 40x40 and 80x80 nodes and the maximum and minimum ϕ values predicted are presented in Table 3 and the results from 40x40 nodes are chosen to show the 3-D perspective plots in Fig. 3. Table 3 shows that the predictions of the maximum ϕ value of the flow field using various flux-limiters are not very different. However, the ability of the schemes in capturing the discontinuities can be observed from the 3-D perspective plots of the solutions in Fig. 3 with the *superbee* limiter giving the best performance in this case.

Table 3 The Maximum and Minimum Field Values of the Square Field Transport Problem

	16x16		32x32		64x64	
	max	min	max	min	max	min
FOU	6.58	0.00	8.60	0.00	9.63	0.00
SOLU:						
van Leer	9.14	0.00	9.99	-7.95×10^{-15}	9.93	-1.65×10^{-12}
minmod	8.41	0.00	9.83	0.00	9.92	0.00
superbee	9.64	-2.74×10^{-7}	10.00	-1.89×10^{-6}	9.95	-1.40×10^{-5}
MUSCL	9.46	-1.01×10^{-7}	9.99	-3.17×10^{-7}	9.94	-3.93×10^{-6}
Koren	9.46	-5.94×10^{-8}	9.99	-2.40×10^{-7}	9.94	-2.69×10^{-6}

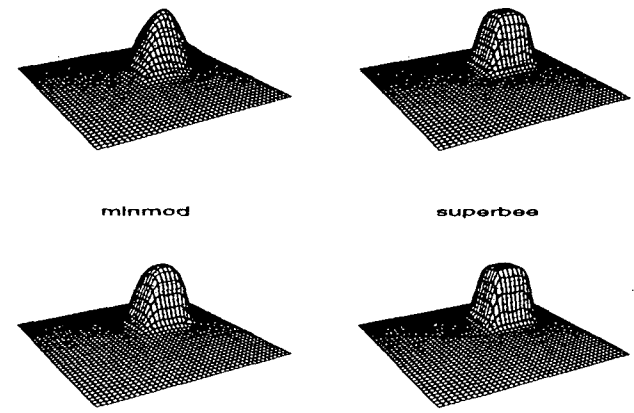

Fig. 3 The 3-D Perspective Plots of the Square Field Transport Proble

3.3 Mixing of a Hot with a Cold Front

A rectangular domain has an initial profile, Fig. 4, of a narrow region of high gradient from top to botto called a "front" which is then twisted by a steady rotational velocity field in a manner similar to that observed on daily weather maps [8]. The initial conditions are defined at t = 0 b

$$\phi(x,y)=-\tanh\left[\frac{y}{2}\cos(ft)-\frac{x}{2}\sin(ft)\right] \tag{18}$$

The domain is $x \ge -4$, $y \le 4$ and

$$f=\frac{1}{r}\frac{f_t}{f_{t\,max}} \tag{19}$$

where f is the frequency, r is the distance from the origin of the co-ordinate system, $f_t = \tanh(r)/\cosh^2(r)$ is the tangential velocity around the centre, and $f_{t\,max} = 0.385$ is the maximum tangential velocity. The expression of the steady velocity field is

$$u(x,y)=-\frac{y}{r}\frac{f_t}{f_{t\,max}}$$

$$v(x,y)=-\frac{x}{r}\frac{f_t}{f_{t\,max}} \tag{20}$$

The initial profile of the scalar field changes gradually from positive values at the bottom boundary to negative values at the top boundary. The solutions presented are after the front has twisted for 4 time units or 400 time steps. Three different grid sizes are used; 16x16, 32x32 and 64x64. The maximum and minimum ϕ values of the flow field are not reported since no scheme introduces oscillation in the solutions in this test proble . However, $\|L\| = \frac{\sqrt{\sum|\phi - \phi_{exact}|^2}}{nx \times ny}$ of 64x64 grid are tabulated in Table 4 to show the relative accuracy of the results using various flux limiters. $\|L\|$ from *superbee* is the lowest indicating that it is the most accurate and similarly *minmod* is the least accurate flux limiter because of its highest $\|L\|$. This is reflected in the contour plots of 64x64 grid in Fig. 5 that the contour plot fro *superbee* is in very good agreement with that from the exact analytical solutions, Fig. 4.

Table 4 $\|L\|$ of the Mixing Test at 64x64 Grid

	$\|L\|$ (x10^{-4})
FOU	11.10
SOLU:	
van Leer	4.53
minmod	6.04
superbee	2.72
MUSCL	3.77
Koren	3.77

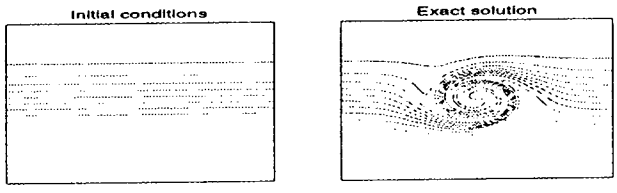

Fig. 4 Contour Plots of the Initial Conditions and Exact Solutions of the Mixing Test

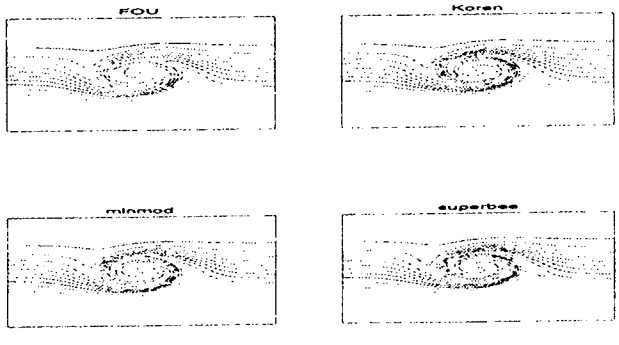

Fig. 5 Contour Plots of the Mixing Test

3.4 Deformation of a Cone-Shaped Scalar Field

The deformation flow problem used here was first defined by Smolarkiewicz [9] and its exact solutions were obtained by Staniforth *et al.* [10]. It is chosen to test the performance of the schemes in highly deformational flow. The steady flow field is defined by the following stream function;

$$\varphi(x, y) = \frac{1}{4\pi}\sin(4\pi x)\cos(4\pi y) \qquad (21)$$

and the two velocity components are derived using u = $-\partial\varphi/\partial y$ and v = $\partial\varphi/\partial x$. Contours of the stream functio and velocity vectors are shown in Fig. 6 and it can be seen that the velocity field is built up from sets of symmetrical counter-rotating vortices, each vertex occupying a square of side 25 units.

Initially, a cone of radius 15 units is centred on the centre of a square domain of side equal to one unit; the origin is specified at the bottom left-hand corner of the square. The problem has an initial condition as in test case 3.1. At t = 0, the cone is in the area of six vortices but its main part is in the area of the two central ones, and then the solutions will be divided into two symmetrical parts which will move inside an area of these two central vortices. Since the fluid elements cannot cross the boundary streamline of the vortex, they cannot escape from the vortex in which they are initially located. Thus, the scalar distribution will be zero over the entire domain except over the six vortices at the centre where it is initially non-zero.

The integration time consists of 2400 time steps of 0.001s, which produces results independent of time step. A grid of 100x100 nodes is used in this test problem and the maximum and minimum values fro each scheme are reported in Table 5 and the isolines of the scalar distribution for various schemes are illustrated in Fig. 7. As in test cases 3.1 and 3.2, the predicted maximum field values are highest using *superbee* and lowest using *minmod* respectively. Again, this agrees with the contour plots of the results in Fig. 7 that the closest agreement with the exact solutions from Staniforth *et al.* [5] is obtained using the *superbee* flux-limiter (the exact solutions are not presented here).

Table 5 The Maximum and Minimum Field Values of the Deformational Flow Proble

	100x100	
	max	min
FOU	1.62	0.00
SOLU:		
van Leer	1.88	$-2.58\text{x}10^{-16}$
minmod	1.77	0.00
superbee	2.10	$-6.11\text{x}10^{-7}$
MUSCL	1.96	$-2.84\text{x}10^{-7}$
Koren	1.94	$-1.05\text{x}10^{-7}$

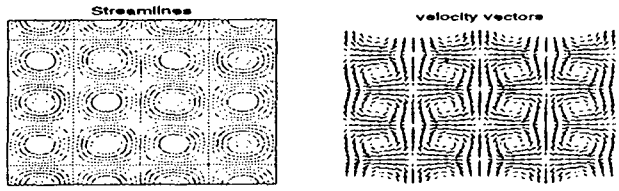

Fig. 6 Contours and Velocity Vectors of the Deformational Flow Problem

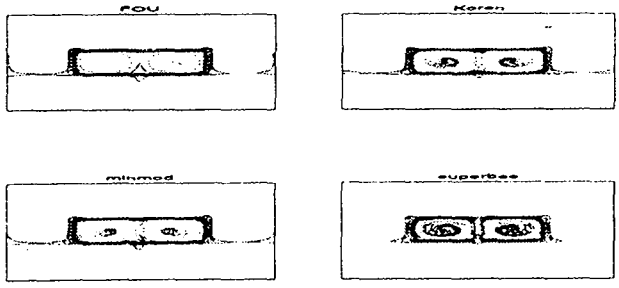

Fig. 7 Contour Plots of the Deformational Flow Problem

3.5 IAHR

This steady problem represents the convection of a step around a curved flow and is used widely to test various differencing schemes. A schematic illustration of the problem is shown in Fig. 8. The velocity field is specified as

$$u(x,y) = 2y(1-x^2)$$
$$v(x,y) = -2x(1-y^2) \qquad (22)$$

and the boundary conditions at the inlet face (for y = 0 and -1 ≤ x ≤ 0) as

$$\phi = 1 + \tanh[10(2x+1)] \qquad (23)$$

A zero normal gradient boundary condition is imposed at the outlet, and at the other faces of the domain, the boundary condition is specified as ϕ =1-tanh(10). This steady-flow problem is treated as unsteady flow, and the solutions are obtained when the ϕ values reach the steady state values, i.e. a pseudo-transient approach. A grid-independent of 71x35 mesh is used in this test case. Fig. 9 shows the variation of ϕ values along the inlet and outlet boundaries of the domain and residuals defined as $\Sigma(\phi^{n+1}-\phi^n)/\phi^{n+1}(\max)$ are plotted in log scale against the number of iterations in Fig. 10.

As in unsteady-flow problems, *superbee* exhibits the best performance in capturing the steep gradient as can be seen at the outlet boundary of the domain in Fig. 9, unfortunately, it shows the worst convergence behaviour, Fig. 10. The flux limiter that shows the best convergence behaviour is *minmod*, however, the solutions from *minmod* are the least accurate, Fig. 9. The compromise, therefore, has to be made between accuracy and convergence. *Koren* is the best choice since its results are close to those using *superbee* and its convergence behaviour is reasonably good.

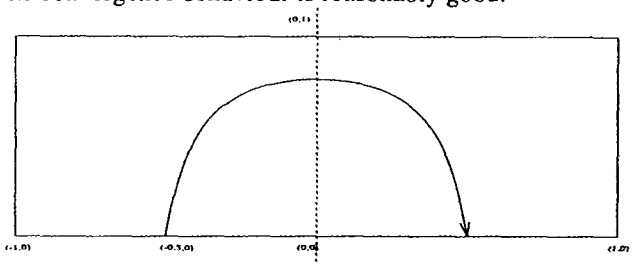

Fig. 8 The Illustration of the Steady-Flow Proble

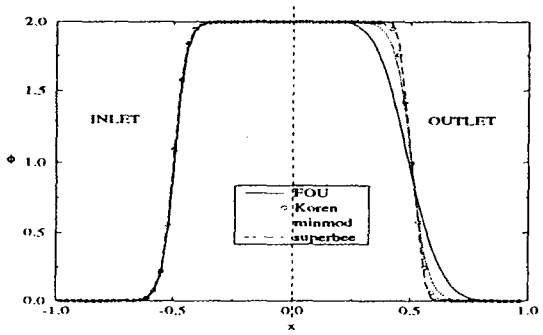

Fig. 9 The Variation of Scalar Value along the Inlet and Outlet Boundaries of the Steady-Flow Problem

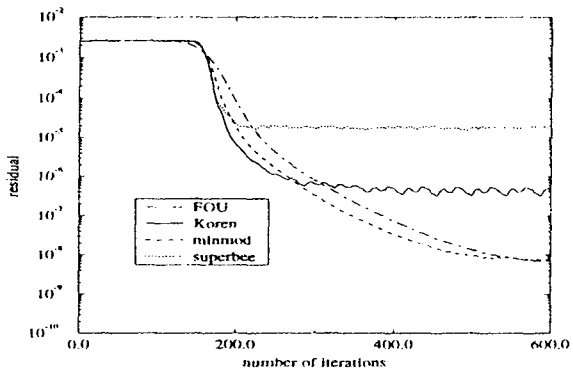

Fig. 10 Residual of Scalar Variable against the Number of Iterations of the Steady-Flow Problem

4. Conclusions

A comparative study, with the focus on the accuracy and convergence behaviour, of five different flux-limiters: *van Leer, minmod, superbee, MUSCL, Koren* basing on a second-order-limited upwind differencing scheme is made using five pure convection steady and unsteady test cases. The most accurate results are obtained using *superbee* flux-limiter whereas *minmod* flux-limiter causes the highest errors in the solutions for all five test cases. Although *superbee* flux limiter shows the best performance in capturing discontinuities in all test cases, its convergence behaviour in steady flow problems is unsatisfactory. Therefore, for the steady-flow problem as in test case 3.5, *Koren* is more appropriate than *superbee* because the accuracy of the results using

Koren is almost as good as *superbee* and *Koren* also has reasonably good convergence behaviour. Whereas the second-order-limited upwind scheme incorporated with *superbee* is the most preferable scheme for the problems with unsteady flow. *Minmod* always gives the positive results unlike the other flux-limiters (Tables 2, 3 and 5), indicating that *minmod* can be used in a wider range of applications.

References

[1] H. K. Versteeg and W. Malalasekera, "An Introduction to Computational Fluid Dynamics: The Finite Volume Method", Longman Group Ltd. , 1995

[2] A. Jameson, W. Schmidt and E. Turkel, "Numerical Solution of the Euler Equations by Finite Volume Method using Runge-Kutta Time-Stepping Schemes", AIAA-81-1259, 14 th AIAA Fluid and Plasma Dynamics Conference, Palo Alto, CA, USA., 1981

[3] B. van Leer, "Towards the Ultimate Conservative Difference Scheme. II. Monotonicity and Conservation Combined in a Second-Order Scheme", Journal of Computational Physics, Vol. 14, 1974, pp. 361-370

[4] P. L. Roe and M. J. Baines, "Algorithms for Advection and Shock Problems", 4th GAMM Conference on Numerical Methods in Fluid Mechanics, Braunschweig, Vieweg, 1982

[5] P. L. Roe, "Some Contributions to the Modelling of Discontinuous Flows", Lectures in Applied Mathematics, Vol. 22, 1985, pp. 163-193

[6] B. van Leer, "Towards the Ultimate Conservative Difference Scheme. V. A Second-Order Sequel to Godunov's Method", Journal of Computational Physics, Vol. 32, 1979, pp. 101-136

[7] B. Koren, "A Robust Upwind Discretization Method for Advection, Diffusion and Source Terms", in C. B. Vreugdenhil and B. Koren (eds), Numerical Methods for Advection-Diffusion Problems, Vieweg, Braunschweig, 1993, pp. 117-137

[8] C. Doswell, "Kinematic Analysis of Frontogenesis Associated with a Nondivergent Vortex", Journal of Atmospheric Sciences, Vol. 41, 1984, pp. 1242-1248

[9] P. K. Smolarkiewicz, "The Multi-Dimensional Crowle Advection Scheme", Monthly Weather Review, Vol. 110, 1982, pp. 1968-1983

[10] A. Staniforth, J. Cote and J. Pudykiewicz, "Comments on Smolarkiewicz's Deformational Flow", Monthly Weather Review, Vol. 115, 1987, pp. 894-900